

# PHOTOGRAMMETRIC APPROACH FOR RETRIEVAL OF CLOUD MOTION AND HEIGHT WITH MISR IMAGERY

Jia Zong and David J. Diner

Jet Propulsion Laboratory, California Institute of Technology  
Mail Stop 169-315  
4800 Oak Grove Drive  
Pasadena, CA 91109 USA

## ABSTRACT

The Multi-angle Imaging Spectro Radiometer (MISR) instrument consists of nine pushbroom cameras pointing at discrete view angles. Multi-angle imagery from MISR creates new opportunities to retrieve scientific parameters related to aerosol, surface, and cloud conditions on the Earth. Cloud top height is one such parameter. In the presence of cloud motion, photogrammetric retrieval of cloud top height has traditionally been considered to be impossible even with stereo imagery. In this paper, we prove that with imaging from orbital altitude and multiple camera view-angles the cloud motion and height are separable. The singularity problem caused by the correlation between cloud motion and height in the image disparity can be resolved under certain mathematical conditions. These require at least three asymmetric MISR cameras used for conjugate cloud image matching and ray intersection. The result provides simultaneous retrieval of cloud top height and cloud motion.

## 1. INTRODUCTION

The Multi-angle Imaging Spectro Radiometer (MISR) instrument for the Earth observing System (EOS) is to be launched in mid 1998 aboard the EOS AM-1 satellite [Diner, et al. 1991]. Its purpose is to study the ecology and climate of the Earth through the acquisition of systematic, global multi-angle imagery in reflected sunlight. The MISR instrument consists of nine pushbroom cameras pointing at nine discrete view angles, arranged with one pointing to nadir, four pointing forward of nadir, and four pointing aftward of nadir (designated as An; Af, Bf, Cf, Df; and Aa, Ba, Ca, Da). Images are acquired with nominal view angles, relative to the reference ellipsoid surface, at angles of  $0^\circ$ ,  $\pm 26.1^\circ$ ,  $\pm 45.6^\circ$ ,  $160.0^\circ$ ,  $\pm 70.5^\circ$  for the An, Af/Aa, Bf/Ba, Cf/Ca, and Df/Da cameras, respectively. Each camera is equipped with four Charge-Coupled Device (CCD) line arrays filtered to provide one of MISR special bands (centered at 446, 558, 672, and 866nm). Each line array consists of 1504 photoactive pix -

els. The overlap swath width of the MISR imaging data (that is, the swath seen in common by all nine cameras) is 360 km, which provides global multi-angle coverage in 9 days at the equator, and 2 days at the poles.

The science data reduction of MISR image is to be conducted at the NASA Langley Data Active Archive Center (DAAC). In the Level 1 standard processing of instrument data, all 36 channels of MISR imagery are radiometrically calibrated and geolocated within a pixel of uncertainty ( $\pm 275$  m) onto two reference surfaces. One called surface *ellipsoid* is defined by the datum of the WGS84 ellipsoid, and the other, called *surface terrain* is defined by a global digital elevation model over land and inland water with WGS84 vertical datum [Jovanovic, 1996] [Zong, 1996]. The geolocated and co-registered multi-band imagery resampled onto a Space-Oblique Mercator (SOM) map projection is then used in the subsequent Level 2 geophysical parameter retrievals. In its Level 2 Top of Atmosphere (TOA)/Cloud processing, cloud classifications and accurate spectral albedos retrieval at a reflecting level reference altitude (RLRA) are among the major MISR science objectives. The RLRA is defined to be the level found by matching features (or areas) with the greatest contrast in the near-nadir viewing directions. Physically, this corresponds to the main reflecting layer, which will typically be the tops of bright clouds, or the surface for clear scenes.

The algorithm for retrieving RLRA is stereophotogrammetric in nature, and makes use of the multiple views from satellite altitude over a wide angular range to separate the effects of wind displacement independently from height. The stereoscopic approach of RLRA retrieval uses radiance images registered at the surface ellipsoid from the Level 1 standard processing and contains two aspects. One is the automatic stereo matching of cloud feature with greatest contrast. Another is the geometric separability of disparity due to cloud motion and height. This paper addresses the second aspect, that is, how to solve the singularity problem embedded in the photogrammetric approach to cloud top height retrieval with possible existence of cloud motion. The main topics of this paper include the effect of cloud motion and height on the image disparity, the mathematical separation condition, the simultaneous cloud motion and height retrieval for the determination of a regional cloud motion field, the cloud height retrieval, some prototype results, and a summary.

## 2. CLOUD IMAGE DISPARITY

According to its definition, the disparity of an object feature is obtained through a stereo matching process of the same feature in images observed from two or more look angles. Physically, disparity is caused by a height difference of an object feature from a fixed point and the motion of the object along the direction where the disparity is measured. In MISR TOA/Cloud processing, the input images are the radiance images registered at the surface ellipsoid. Therefore, a cloud above the ellipsoid surface causes an image disparity shown in Figure 1a

$AR^*$ , where A and  $B_1$  represent the conjugate image features of a cloud edge.

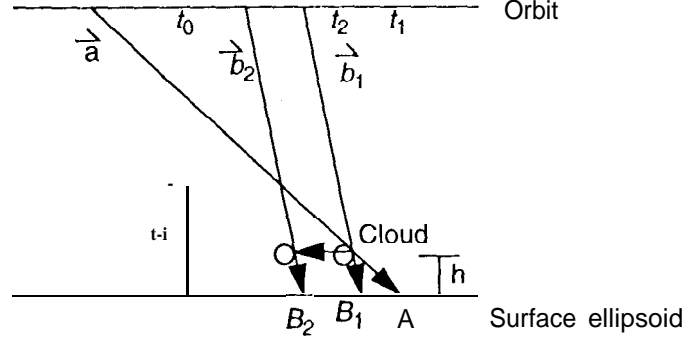


**Figure 1. Disparity of cloud edge in two images with different view angles**

In the absence of cloud motion, the cloud height can be obtained from intersecting conjugate look rays  $\vec{a}$  and  $\vec{b}_1$ . If the cloud also has a velocity component along the flight direction, the disparity  $\overline{AB}_2$  is then caused by the combined effect from both the cloud height and the cloud motion. Directly intersecting look rays  $\vec{a}$  and  $\vec{b}_2$  would result in an incorrect cloud height  $h'$ . In order to obtain accurate values of RLRA, it is necessary to separate the disparities due to cloud advection from those due to cloud height.

### 3. SEPARATION CONDITION

Figure 2 shows the geometry of MISR imaging in the along-track direction where cloud height and motion are highly correlated due to large view angle difference from one camera to another. The shaded circles indicate the locations of a cloud at different times  $t_i$ , assuming there is a constant along-track cloud motion  $v_c$ . The projections of the cloud onto the surface ellipsoid are at the locations  $x_i$  at these times, with the discrete MISR camera view angles  $\theta_i$ . For simplicity in this discussion, the cloud motion and the camera look vectors are assumed to lie in the along-track plane. The actual algorithm employed takes into account the cross-track component of both the camera look vectors and the cloud motion.

If a cloud edge is seen by two cameras with different view angles at times  $t_1$  and  $t_2$ , respectively, then the traveling distance of the spacecraft and that of the cloud during this time interval can be described by the following equations:

$$v_s(t_2 - t_1) = (R + H)(\alpha_2 - \alpha_1) - (R + H)(\Gamma_2 - \Gamma_1) \quad (1)$$

$$v_c(t_2 - t_1) = (R + h)(\alpha_2 - \alpha_1) - (R + h)(\gamma_2 - \gamma_1) \quad (2)$$

where  $v_s$  and  $v_c$  are the velocities of the spacecraft and the cloud in the along-track direction, respectively,  $R$  is the radius of the Earth,  $H$  is the orbit altitude above the Earth's surface, and  $h$  is the cloud height. As shown in Figure 2,  $\alpha_1$  and  $\alpha_2$  are the angles between the initial radial line at the time  $t_0$  and the radial line passing the image locations  $x_1$  and  $x_2$ , respectively;  $\Gamma_1$  and  $\Gamma_2$  are the angles between the radial lines to the spacecraft and the corresponding image locations  $x_1$  and  $x_2$ ; and  $\gamma_1$  and  $\gamma_2$  are the angles between the radial lines to the cloud and the corresponding image locations  $x_1$  and  $x_2$ .

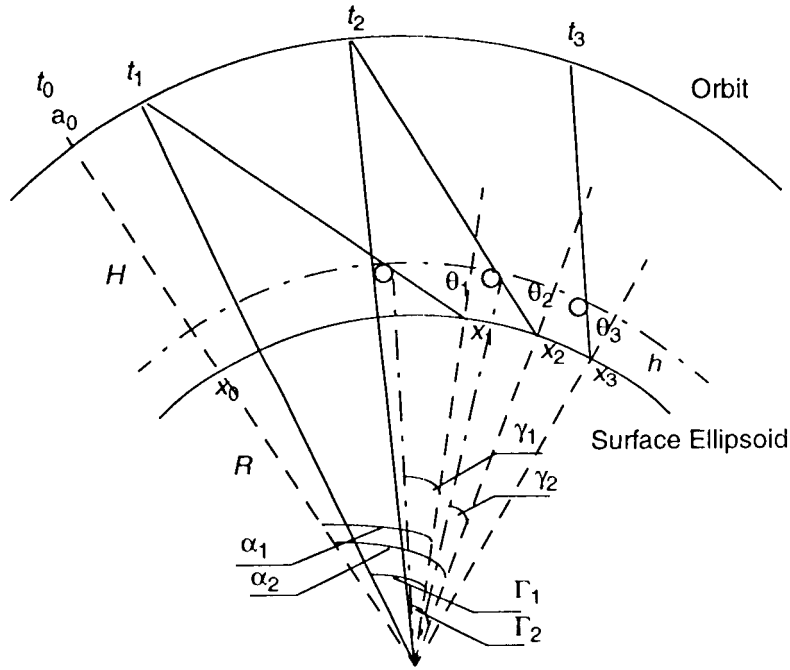


**Figure 2. Geometry of MISR imaging of cloud in the along-track direction**

Since  $h \ll R$ , Eq. (2) can be rewritten with variables that we are interested in:

$$v_c(t_2 - t_1) = (x_2 - x_1) + h(\tan \theta_1 - \tan \theta_2) \quad (3)$$

With multi-angle images, Eq. (3) can be generalized into a linear system as

follows:

$$\begin{aligned} v_c(t_j - t_i) - h(\tan\theta_i - \tan\theta_j) &= (x_j - x_i) \\ (i, j &= 1, 2, \dots, n, i \neq j, n \geq 3) \end{aligned} \quad (4)$$

The linear system expressed by Eq. (4) represents a straight line in the  $Ax$  versus  $At$  space in which each matching pair contributes a point to this line, where  $v_c$  and  $h$  can be determined from the slope and intercept of the line. Matching at least three images with different view angles  $\theta_i$  are required to solve for  $v_c$  and  $h$ . In addition, any two linear equations are dependent on each other if their determinant is zero, i.e., if

$$\det A = (t_i - t_{i-1})(\tan\theta_i - \tan\theta_{i+1}) - (t_{i+1} - t_i)(\tan\theta_{i-1} - \tan\theta_i) = 0 \quad (5)$$

In such a case,  $v_c$  and  $h$  are inseparable from these two equations. On a small scale where the flight line is straight and the surface is a plane, this singularity will always be true. On an orbital scale with a circle or an elliptic orbit and a spheroid or an ellipsoidal surface, the traveling time interval between a pair of cameras does not linearly relate to the tangent of view angles as depicted in Figure 2 and represented in Eq. (1), as long as the selected camera view angles do not happen to be symmetric around the nadir view.

#### 4. CLOUD MOTION AND HEIGHT RETRIEVAL

In MISR TOA/Cloud processing, we assume that vertical cloud motion can be ignored during the 7 minute time interval between camera Df and Da views, and that the horizontal cloud motion at a given altitude is constant during this period of time over a domain size of -100 km. By selecting a set of cameras with non-symmetric and oblique view angles, we are able to separate the heights and velocities in the data reduction. In order to determine the regional cloud field, a feature-based matching algorithm is used to simultaneously retrieve velocity and height values for a sparse subset of features in the MISR imagery. The algorithm is first applied to the Df, Bf, and An cameras to detect the image disparity values [David, i 997]. The cloud height and motion of each point from this subset is determined by intersecting the three-dimensional conjugate look rays obtained from image matching. The algorithm is applied independently to the Da, Ba, and An cameras. The results are combined to generate the final cloud motion field.

Assume that there is no vertical cloud motion but only a constant horizontal cloud motion. Then, the cloud motion vector, the conjugate look rays from im-

age matching of D, B, and An cameras, and the surface disparities resulting from the matching should form a closed loop in a three-dimensional Cartesian coordinate system as shown in Figure 3.

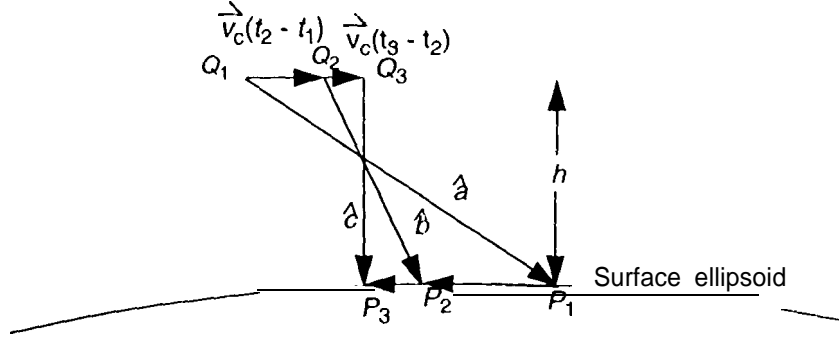


**Figure 3. Ray intersection to retrieve cloud motion**

The following vector equations represent this relationship:

$$\overrightarrow{P_1 P_2} = \lambda_2 \hat{b} + \vec{v}_c(t_2 - t_1) - \lambda_1 \hat{a} \quad (6)$$

$$\overrightarrow{P_2 P_3} = \lambda_3 \hat{c} + \vec{v}_c(t_3 - t_2) - \lambda_1 \hat{b} \quad (7)$$

where  $P_1, P_2,$  and  $P_3$  are the three-dimensional ground points obtained from image matching, representing conjugate image locations of the same cloud edge on the surface ellipsoid;  $\hat{a}, \hat{b},$  and  $\hat{c}$  are the known unit vectors of the conjugate look rays; and  $\lambda_1, \lambda_2,$  and  $\lambda_3$  are the unknown scale factors of the look rays for them to intersect with the cloud, respectively. For each set of 3 conjugate look rays, the six unknowns, describing the cloud motion by the velocity  $v_c$  and the cloud locations by the ray vector scale factors  $\lambda_1, \lambda_2,$  and  $\lambda_3$ , can be solved simultaneously with these six equations. However, in order to easily impose the condition  $v_{cz} = 0$  (no vertical motion) into Eqs. (6) and (7), it is preferable to represent this relationship in a local coordinate system where its z-axis is aligned with the zenith direction at nadir image point  $P_3$ . The x-axis and the y-axis can be defined as the along-track and the cross-track directions, respectively. Because of the condition  $v_{cz} = 0$ ,

$$\begin{cases} \lambda_2 = \frac{(z_2 - z_1)}{z} + \frac{a_z}{b} \lambda_1, \\ \lambda_3 = \frac{(z_3 - z_1)}{c} + \frac{a_z}{c} \lambda_1 \end{cases} \quad (8)$$

Equations (6) and (7) can be decomposed into a set for along-track (9) and another set for cross-track (10):

$$\begin{cases} x_2 - x_1 = v_{cx}(t_2 - t_1) + \frac{b}{b_z} x (z_2 - z_1) - \lambda_1 \left( a_x - b \frac{a_z}{b_z} \right) \\ x_3 - x_1 = v_{cx}(t_3 - t_2) + \frac{c}{c_z} x (z_3 - z_1) - \frac{b}{b_z} x (z_2 - z_1) - \lambda_1 \left( b \frac{a_z}{b_z} - c \frac{a_z}{c_z} \right) \end{cases} \quad (9)$$

$$\begin{cases} y_2 - y_1 = v_{cy}(t_2 - t_1) + \frac{b}{b_z} y (z_2 - z_1) - \lambda_1 \left( a_y - b \frac{a_z}{b_z} \right) \\ y_3 - y_1 = v_{cy}(t_3 - t_2) + \frac{c}{c_z} y (z_3 - z_1) - \frac{b}{b_z} y (z_2 - z_1) - \lambda_1 \left( b \frac{a_z}{b_z} - c \frac{a_z}{c_z} \right) \end{cases} \quad (10)$$

Equations (9) and (10) are equivalent to Eq. (4), but generalized to three dimensions. Since there are four equations and three unknowns ( $\lambda_1, v_{cx}, v_{cy}$ ), the problem is overdetermined and the equations are solved by least-squares.

The solutions of Eqs. (9) and (10) provide directly the cloud velocity  $\vec{v}_c$  and look ray scale factor  $\lambda_1, \lambda_2$ , and  $\lambda_3$ . The height of the cloud of this matched triplet is obtained by projecting the nadir view look ray, e.g.  $\lambda_3 \hat{c}$ , onto the normal direction at the surface ellipsoid where the look ray intersects:

$$h = \lambda_3 \hat{c} \cdot \hat{n} \quad (11)$$

## 5. CLOUD HEIGHT RETRIEVAL

Cloud motion is typically homogeneous over a larger area than cloud height. The algorithm to provide the disparities which as input to motion retrieval equations only need to find good matches for a sparse array of points over the - iOO

km dimension. However, the height field is desired at higher resolution (a few km) with contiguous spatial coverage. Thus, a different approach to height retrieval is required. Once the regional motion field has been derived, it serves to provide a cloud motion correction in the conversion of the fine resolution disparities to heights. The high resolution image disparity field is derived with an area-based matching algorithm applying to two pairs of near-nadir cameras Af-An and Aa-An [David, 1997]. The ray intersection of conjugate image rays is done with a modified version of minimum distance intersection to be discussed in this section. The resulting cloud height retrieval (based on Af-An and As-An results) is used to establish RLRA.

Ray intersection with minimum distance intersection is a simple algorithm. As shown in Figure 4 (a), it considers the errors associated with camera look rays and errors introduced during the processing of image co-registration and image matching, and determines the minimum distance vector  $\hat{d}$  between two conjugate look rays  $\hat{a}$  and  $\hat{b}$  as:

$$\hat{d} = \hat{a} \times \hat{b} \quad (12)$$

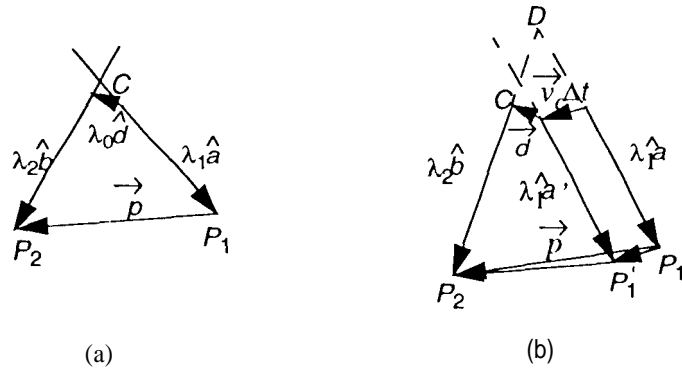


Figure 4. Minimum distance of conjugate rays with and without motion

If  $\hat{p}$  denotes the vector connecting the two ground points  $P_1$  and  $P_2$  on the surface ellipsoid from image matching, then the four vectors  $\hat{p}$ ,  $\lambda_2 \hat{b}$ ,  $\lambda_1 \hat{a}$ , and  $\lambda_0 \hat{d}$  must close, where  $\lambda_0$ ,  $\lambda_1$ , and  $\lambda_2$  are the scale factors to the corresponding vectors. That is,

$$\hat{p} = \lambda_2 \hat{b} + \lambda_0 \hat{d} - \lambda_1 \hat{a} \quad (13)$$

Equation (13) contains totally 3 individual equations and 3 unknowns  $\lambda_0$ ,  $\lambda_1$ , and  $\lambda_2$ , for each pair of conjugate rays and each intersecting point. Therefore, the

intersecting object point can be obtained starting from the nadir image location, say  $P_2$ :

$$C = P_2 - \lambda_2 \hat{b} - \frac{1}{2} \lambda_0 \hat{d} \quad (14)$$

Now consider that the cloud moves with velocity  $\vec{v}_c$  (horizontally in two dimensions) during the period  $\Delta t$  between the conjugate cloud features were seen by the two involved cameras. As shown in Figure 4 (b),  $\hat{d}'$  is the look vector as if there is no cloud motion, and  $\hat{d}$  is the real look vector due to the existence of cloud motion  $\vec{v}_c \Delta t$ . If we directly intersect the two look vectors  $\hat{d}$  and  $\hat{b}$ , the intersection will be around point  $D$  at a wrong height. To remove the cloud motion effect, we assume the cloud was actually seen by another look vector  $\hat{d}'$  parallel to  $\hat{d}$  at another ground position  $P_1'$  by the forward camera at the time  $t_p$ . Then Eq. (13) becomes:

$$\hat{p} - \vec{v}_c \Delta t = \lambda_2 \hat{b} + \lambda_0 \hat{d}' - \lambda_1 \hat{a} \quad (15)$$

Similar to Eq. (13), there are 3 equation and 3 unknowns  $\lambda_0$ ,  $\lambda_1$ , and  $\lambda_2$  for each pair of conjugate rays and each intersecting point. The three-dimensional location of the cloud can be obtained just as is done with Eq. (14) after the minimum distance intersection with motion is determined using Eq. (15).

## 6. PROTOTYPE RESULT

A prototype algorithm was implemented to prove the separability of cloud and cloud motion with MISR data. A number of test cloud features were simulated at the left, center, and right location for a swath line, and several such lines were simulated. Each test cloud was assumed at an altitude of 0 m, 550 m, 1 km, 3 km, 5 km, or 10 km above the surface ellipsoid with a velocity of 0 m/s, 12 m/s, 24 m/s, or 48 m/s in either the along-track, cross-track, or any diagonal direction. Since TOA/Cloud processing retrieves cloud motion and height with MISR image data registered at the surface ellipsoid, the locations of test cloud features in the surface ellipsoid projected MISR image were simulated according to simulated MISR orbit and camera data.

Table I shows the test result. The first column is the MISR camera triplet used for simultaneous cloud motion and height retrieval. The determinants of these camera combination are in the next column according to Eq. (7). The cloud motion and height from ray intersection results are listed in the remaining columns. Here,  $\sigma_{diff}$  represents the standard deviation of the retrieval values from

the known “true” value, and  $Max_{diff}$  is the largest error observed. For asymmetric camera combinations An-B f-Df and Aa-Bf-Df, the maximum cloud motion deviation is less than 1 m/s from the “true” value and maximum cloud top height deviation is less than 60 m. On the other hand, for symmetric camera triplets An-Bf-Aa and An-Bf-Aa, their determinants are too close to zero to provide reliable retrievals. The test confirmed our selection of the D, B, and An camera triplets for the stereoscopic retrieval of cloud motion. In case any default camera does not provide good image data, an alternative camera set that passes the determinant test will be used.

Table 1: Cloud Motion Retrieval Test Results

| Camera Triplet | $detA$ (line) | $\Delta v_{cx}$ (m/s) |              | $\Delta v_{cy}$ (m/s) |              | Ah (m)          |              |
|----------------|---------------|-----------------------|--------------|-----------------------|--------------|-----------------|--------------|
|                |               | $\sigma_{diff}$       | $Max_{diff}$ | $\sigma_{diff}$       | $Max_{diff}$ | $\sigma_{diff}$ | $Max_{diff}$ |
| An-Bf-Df       | -1229.7       | 0.35                  | 0.89         | 0.03                  | 0.08         | 22.1            | 53.5         |
| Aa-Bf-Df       | -1891.6       | 0.36                  | 0.88         | 0.03                  | 0.09         | 26.0            | 60.8         |
| An-Bf-Aa       | -40.7         | 0.92                  | 2.96         | 0.15                  | 0.49         | 84.5            | 268.0        |
| An-Bf-Ba       | -6.1          | 12.2                  | 36.5         | 1.72                  | 5.08         | 1102.9          | 3284.5       |

## 7. SUMMARY

On an orbital scale with imaging at multiple view angles, it is possible to simultaneously retrieve cloud motion and height using a stereoscopic approach. By using non-symmetric MISR cameras, including the most oblique ones, we are able to avoid mathematical singularity and obtain accurate retrievals.

## 8. ACKNOWLEDGMENTS

The authors gratefully acknowledge the efforts of Roger Davies, John V. Martonchik, and Jan-Peter Muller of the MISR Science Team, and Earl G. Hanson and Velkjo M. Jovanovic of the MISR Science Data System Team. This research is being carried out at the Jet Propulsion Laboratory, California Institute of Technology, under contract with the National Aeronautics and Space Administration.

## 9. REFERENCE

Diner, D. J., Bruegge, C. J., Martonchick, J. V., Bothwell, G. W., Danielson, E.

D., Floyd, E. L., Ford, V. G., Hovland, L. E., Jones, K. L., and White, M. L., A Multiangle Imaging Spectroradiometer for Terrestrial Remote Sensing from the Earth-Observing System, International Journal of Imaging Systems and Tech, 1991

Diner, D. J., Davies, R., DiGirolamo, L., Moroney, C., Muller, J-P., Paradise, S. R., Wenkert, D., Zong, J., Level 2 Cloud Detection and Classification Algorithm Theoretical Basis, JPL internal document D- 11399, Rev, B, 1997

Jovanovic, V. M., Smyth, M. M., and Zong, J., Autonomous and Continuous Georectification of Multi-angle Imaging Spectro-Radiometer (MISR) Imagery, ISPRS Int. Arch. of Photogrammetry, vol. XVIII, Commission III, Vienna, 1996

Zong, J., M.M. Smyth, and Veljko M. Jovanovic. MISR band-to-band registration. In Multispectral Imaging for Terrestrial Applications. Proc. SPIE 2818, Denver, Co, 5-9 August, 1996